Origin of laser-induced internal cooling of Yb^{3+}-doped systems

J. Fernández[a,b,c], A. Mendioroz[a], R. Balda[a,b,c], M. Voda[c], M. Al-Saleh[a] , A. J. García-Adeva[d], J. L. Adam[e], and J. Lucas[e]

[a]Dpto. Fisica Aplicada I, Escuela Superior de Ingenieros, Alda. Urquijo s/n 48013 Bilbao (Spain)

[b]Centro Mixto CSIC-UPV/EHU, [c]Donostia International Physics Center (DIPC), Basque Country (Spain)

[d]Structure/Property Relation Group (MST-8), Los Alamos National Lab, NM 87545, USA

[e]Lab. de Verres et Céramiques, Université de Rennes I, UMR-CNRS 6512, Campus de Beaulieu, 35042 Rennes, Cedex, France

Keywords: Optical properties, Ytterbium, Laser cooling, Electron-phonon interactions.

ABSTRACT

Laser induced internal cooling has been investigated in a new fluorochloride glass (CNBZn) and a fluoride glass (BIG) doped with $2.1x10^{20}$ Yb^{3+} ions/cm^3 and in a KPb_2Cl_5 crystal doped with $5x10^{19}$ Yb^{3+} ions/cm^3 by using collinear photothermal deflection and conventional laser excitation spectroscopies under high photon irradiances. The cooling efficiency for CNBZn glass which is ~2.0 % relative to the absorbed laser power at 1010 nm and 300 K falls about 20% at 77 K. The cooling efficiency for BIG glass was only ~0.6% at room temperature. For the Yb^{3+} doped KPb_2Cl_5 crystal we have shown internal laser cooling with a cooling efficiency of about 0.2% at room temperature. This is the third ytterbium-doped crystal, after $KGd(WO_4)$ (Ref.10) and YAG (Ref.11), in which anti-Stokes laser-induced internal cooling has been demonstrated. The observed temperature dependence of the cooling process can be explained by a simple model accounting for the photon-ion-phonon interaction.

1. INTRODUCTION

In 1929 Pringsheim [1] suggested the possibility of cooling matter by anti-Stokes fluorescence. In 1995, the first experimental evidence of laser cooling in a solid, an Yb^{3+} doped fluorozirconate glass, was presented by Epstein et al. [2]. From then on, several works have been published regarding topics as the composition requirements of the matrices to achieve cooling [3-5] or the temperature drop attainable in fiber configuration [6-8]. Recently, some of the authors of this work have demonstrated laser cooling in a new ytterbium doped fluorochloride glass [9]. Throughout the last year laser cooling was observed in ytterbium-doped $KGd(WO_4)_4$ [10] and YAG [11] crystals for the first time. Moreover, cooling has also been observed in liquids [12] and semiconductors [13].

Among the potential applications of anti-Stokes laser cooling of solids, two main fields seem to attract the interest on this effect: cryocoolers for aerospatial applications and high power solid state lasers in which no excess heat is generated.

The low temperature cooling efficiency of glasses has been investigated in two fluorozirconate glasses and a phosphate glass [4] by measuring the absorption and emission spectra of the samples at different temperatures and evaluating the

Corresponding author: email:wupferoj@bi.ehu.es; Phone: 34 94 601 4044; Fax: 34 94 601 4178

Rare-Earth-Doped Materials and Devices VI, Shibin Jiang, Robert W. Keys, Editors,
Proceedings of SPIE Vol. 4645 (2002) © 2002 SPIE · 0277-786X/02/$15.00

cooling efficiencies when pumping the sample at a wavelength which corresponds to an absorption coefficient of 10^{-3} cm^{-1}. The results reveal the BIGaZYbTZr (BaF_2-InF_3-GaF_3-ZnF_2-ThF_4-ZrF_4) glass as the best candidate, being twice as efficient as ZBLAN glass at 50 K. Theoretical studies on the capability of rare-earth doped glasses as low temperature coolers [14] point-out to an actual ability of the studied glass (Yb^{3+}-doped ZBLAN glass) to work as a cryocooler. On the other hand, the technical problems such as laser losses, luminescence efficiency, evacuation of luminescent light, adequate path lengths, high optical quality of components, suitable laser sources etc., seem to be surmountable.

Regarding the second field of interest, Bowman [15] proposed to use radiation cooling by anty-Stokes fluorescence within the laser medium to balance the heat generated by the Stokes shifted stimulated emission (radiation balanced lasers). This could arise in very high power lasers in which limitations in beam quality and average power could be overcome. The studies carried-out by Bowman and Mungan to evaluate Ytterbium doped laser materials for their utility in radiation balanced laser systems [16, 10] predict that Yb^{3+} doped $KY(WO_4)_2$ and $KGd(WO_4)_2$ crystals will show the highest performance in this kind of systems. In these studies, fluorescence optical cooling in $KGd(WO_4)_2$ crystal has been reported for the first time, which opens a very encouraging outlook for radiation balanced lasers.

In this work, we present the experimental evidences of laser cooling in two bulk Yb^{3+}- doped fluorochloride and fluoride glasses together with the first results on internal laser cooling in a new ytterbium-doped KPb_2Cl_5 crystal. These results have been obtained by using two different techniques: collinear photothermal deflection spectroscopy and conventional laser excitation spectroscopy performed under the same high photon irradiances. The photothermal measurements give for these glasses similar results to those found in fluorozirconate glass and show similar cooling efficiencies. For the crystal the cooling efficiency is a little lower due to the small amount of Yb^{3+} ions that is allowed to enter the crystal lattice. On the other hand, the spectroscopic results clearly reveal that the cooling range is restricted to a narrow spectral region which depends on the phonon density of states of the material. Moreover, the thermal dependence of the additional fluorescence which appears in the excitation spectra as a consequence of cooling, makes clear that the cooling efficiency is a function of temperature.

2. EXPERIMENTAL

2.1 CNBZn and BIG glasses

Two samples of CNBZn glass (CdF_2-$CdCl_2$-NaF-BaF_2-$BaCl_2$-ZnF_2) and BIG (BaF_2-InF_3-GaF_3-ZnF_2-LuF_3-GdF_3) glass doped with 1 mol % of YbF_3 were investigated. The samples of dimensions 2x8x10 mm^3 were suspended from a silk wire cross inside a cryostat evacuated to ~ 10^{-2} mbar to improve thermal isolation. Figure 1 shows a block diagram of the experimental set-up. The beam of a tunable (λ= 905 to 1090 nm) cw titanium-sapphire ring laser (8 GHz bandwidth) which entered the sample perpendicularly to the center of the 2x8 mm face was modulated at 1.24 Hz by means of a mechanical chopper. A fraction of the incident power was utilized for signal normalization. A copropagating helium-neon probe laser beam (λ= 632.8 nm) was co-aligned with the pump beam through a dichroic element. Both pump and probe copropagating beams were focused into the middle of the sample with diameters of ~ 100 μm and ~ 60 μm respectively. After leaving the sample, the beams passed through a second identical lens separated from the first one by a distance twice the focal length (5 cm) to avoid high divergence of the emerging beams. A second dichroic beam splitter deviated the pumping beam to a pyroelectric detector which measured the transmitted pumping power. Before reaching a quadrant position detector the probe beam passed through an interference filter to eliminate residual pumping radiation. The excitation spectra were measured with the same configuration by collecting the fluorescence at a right-angle from the focused area of the pumping beam by means of a collimating lens, and focusing it with a second lens at the 100 μm entrance slit of a 0.22 m monochromator provided with an extended infrared photomultiplier. Lock-in detection was used in both experiments. Thermal deflection waveforms were detected by using a digital scope.

2.2 KPb_2Cl_5 crystal

Single crystals of non-hygroscopic Yb^{3+} doped KPb_2Cl_5 crystal, typically 3 cm long and 2 cm in diameter, have been grown by the Bridgman technique in our laboratory, in chloride atmosphere with a two-zone transparent furnace, a

temperature gradient of 18 °C/cm and 1 mm per hour growth rate. Quartz ampoules with a pointed end were used to serve as seed selector and promote single crystal growth. The Yb^{3+} content was about 5 x 10^{19} ions/cm^3. A plate with dimensions of 4.6x4x3.3 mm^3 was cut from block and adequately polished for spectroscopic measurements.
The experimental set-up for the thermal deflection and spectroscopic measurements of this crystal was the one described before for the glass samples.

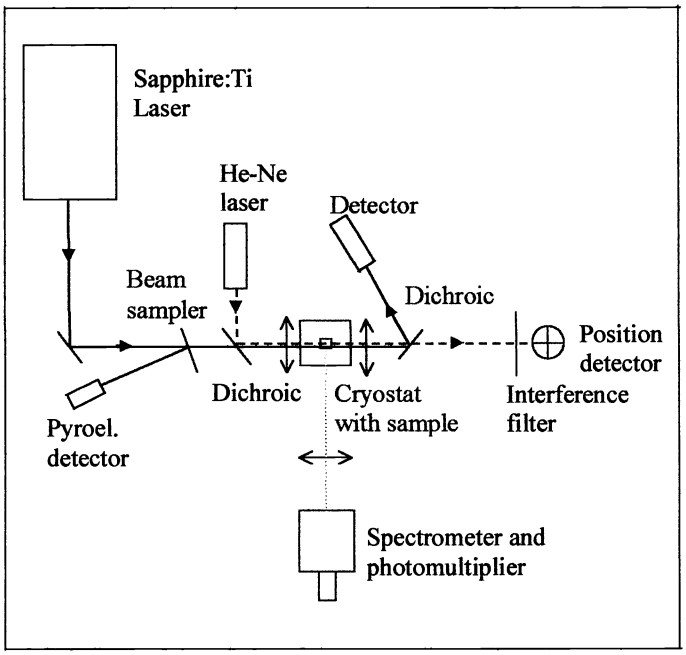

Figure 1. Block diagram of the experimental set-up used in the photothermal deflection, absorption, and excitation measurements.

3. RESULTS

3.1. Photothermal quantum efficiency measurements

The calculation of the Quantum efficiency (QE), both in glass and crystal samples, was carried-out by considering a simplified model of the Yb^{3+} ions as a two level system (figure 2). We shall consider a typical process in which a photon of energy $\hbar\omega_L$ from the incident beam of intensity I_0 modulated at a frequency of ω_m is absorbed by an electron that goes up to the excited state. The relaxation to the ground state can take place through radiative or non-radiative processes with probabilities W_R and W_{NR} respectively, at a mean energy of $\hbar\omega_0$. The energy difference between the incident and fluorescent photons is exchanged as heat with the host.

In this model, the heat the sample exchanges per unit time and unit volume in a typical heating process is

$$H = n_2\left[W_{NR}\hbar\omega_L + W_R\hbar(\omega_L - \omega_0)\right] \qquad (1)$$

where n_2 is the population density of the excited state.

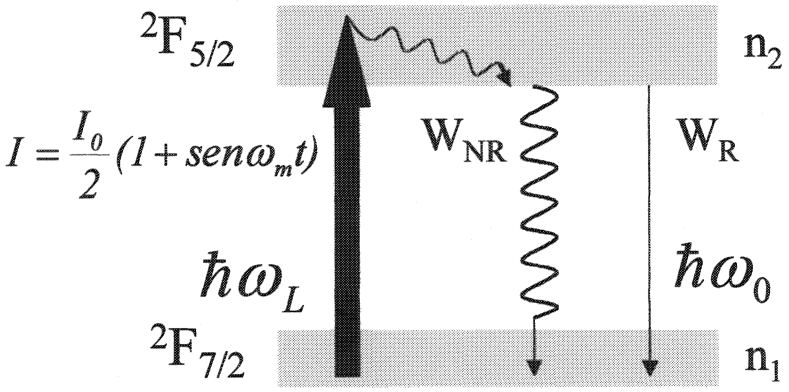

Figure 2. Two level scheme of the Yb^{3+} ions in a typical heating process.

The excited state population is governed by the incident beam modulation frequency ω_m and the lifetime of the level, τ.

$$\frac{dn_2}{dt} = n_1 \frac{\sigma I}{\hbar\omega_L} - \frac{n_2}{\tau} \tag{2}$$

where σ is the absorption cross section and n_1 is the population of the ground state.

If we solve this equation and enter the result in equation 1, we find the following result [17],

$$H(\omega) = \frac{I_0}{2} n_1 \sigma \left(1 - \eta \frac{\omega_0}{\omega_L}\right) \cos\Phi \; sen(\omega_m t + \Phi) \tag{3}$$

where $\Phi = tan^{-1}(\omega_m \tau)$ is the phase relative to the incident modulation beam.

In the case of low modulation frequency, $\tau\omega_m << 1$ the heat the sample exchanges per unit time and unit volume takes a very simple form,

$$H = n_1 \sigma I_0 \left[1 - \eta \frac{\omega_0}{\omega_L}\right] \tag{4}$$

where η is the fluorescence QE of the excited state, that is defined as the ratio of the radiative relaxation probability to the total relaxation probability:

$$\eta = \frac{W_R}{W_R + W_{NR}} = W_R \tau$$

In this collinear configuration, the amplitude of the angular deviation of the probe beam is always proportional to the amount of heat the sample exchanges, whichever its optical or thermal properties are [18]. This allows to relate the

amplitude of the deflection at each wavelength to the typical relaxation parameters of the Yb^{3+} ions after the absorption of the pumping radiation, in particular to the QE of the $^2F_{5/2} \rightarrow {}^2F_{7/2}$ transition, giving thus,

$$\frac{PDS}{n_1 \sigma I_0} = C\left[1 - \eta \frac{\omega_0}{\omega_L}\right] = C\left[1 - \eta \frac{\lambda_L}{\lambda_0}\right] \qquad (5)$$

As can be seen the normalized photothermal deflection signal divided by the absorption of the sample has a linear dependence with the pumping wavelength. From the slope and intercept of this straight line, and by using the value of the mean fluorescence wavelength (at which the zero deflection signal occurs), the QE η can be obtained.

3.2. Quantum efficiency measurements in CNBZn and BIG glasses

The lock-in phase and amplitude of the photothermal deflection, normalized by the absorption, for the CNBZn sample, are displayed in Fig. 3 as a function of the pumping wavelength. As predicted by theory [19], a neat change of about 180°, can be observed during the transition from the heating to the cooling region, at around 988 nm (Fig. 3(a)). The QE in the heating region as measured from the photothermal amplitude and absorption [17,18] was 0.996 and the one at the beginning of the cooling region (from 988 nm to 1010 nm), 1.016. Therefore, the cooling efficiency estimated by using the QE measurements is about 2.0 %. In the case of BIG glass, the estimated cooling efficiency (983-1010 nm region) was only 0.6 %. It is worthy to notice the nonlinear dependence of the photothermal deflection amplitude with the pumping wavelength in the whole cooling region. This behavior impedes photothermal QE measurements at wavelengths longer than 1010 nm. As we shall see in the next section, this broad peak formed by the photothermal deflection approximately resembles the one observed for the excess of luminescence associated with cooling, thus confirming the nonlinear behavior of this process.

3.3. Quantum efficiency measurements in KPb_2Cl_5 crystal

The room temperature photothermal deflection signal waveforms of KPb_2Cl_5 crystal recorded in the scope for different pumping wavelengths are shown in fig. 4. The zero signal occurs around 985 nm. The lock-in phase and amplitude of the photothermal deflection, normalized by the absorption, are displayed in fig. 5 as a function of the pumping wavelength. As can be seen, the cooling region is sharply defined by a 180° phase jump around 985 nm (fig. 5(a)). The measured QE in the heating region was 0.995 and the one at the beginning of the cooling range, 0.997. Therefore, the cooling efficiency estimated by using the QE measurements is about 0.2 %. As in the glass samples, a nonlinear dependence of the photothermal deflection amplitude with the pumping wavelength in the whole cooling region can be observed.

3.4. Cooling investigations by excitation spectra

3.4.1 CNBZn and BIG glasses

To further investigate the origin of the observed cooling, we performed excitation measurements in both samples at different pumping photon irradiances and temperatures by keeping the system in the same conditions. As an example, fig. 6(a) shows the excitation spectra measured at 225 K for the CNBZn glass collecting the luminescence at 1040 nm (at the end of the cooling zone) and at two different pumping irradiances, 880 and 150 mW. Figure 6(b) displays the normalized difference of both spectra. As we can see, except for the zone around the main absorption peak where an accurate difference is difficult to obtain (probably due to some saturation in the spectrum taken at high irradiances), the difference mainly consists of a broad peak (shaded region in fig. 6(b)) which covers the spectral range where cooling occurs. This new peak must correspond to a fluorescence excess produced as a consequence of the cooling process which allows for an additional population of the excited state in this region. This means that at high photon irradiances, other than first order processes are playing a principal role in this spectral range.

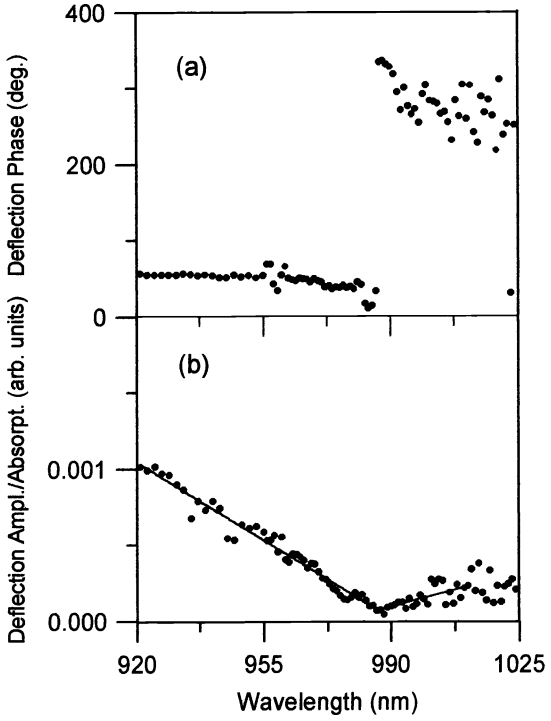

Figure 3. (a) Phase of the photothermal deflection signal and (b) photothermal deflection amplitude (normalized by the incident laser power) divided by the absorption of the CNBZn glass sample.

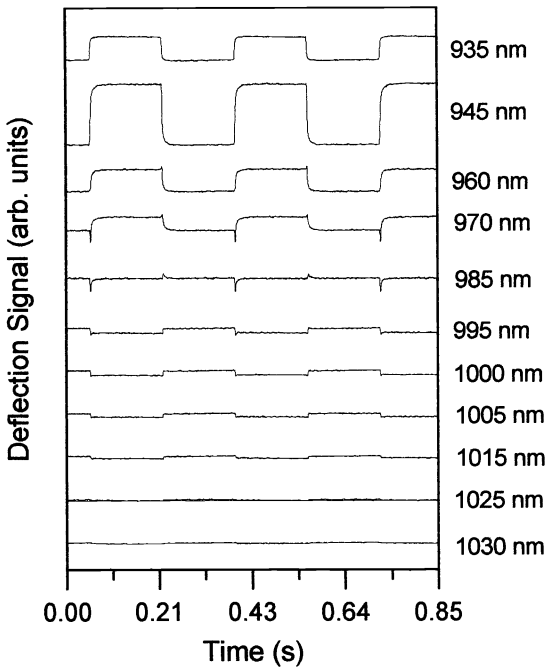

Figure 4. Photothermal deflection signal waveforms obtained for the KPb_2Cl_5 crystal at room temperature.

3.4.2 KPb_2Cl_5 crystal

The cooling process and estimation of cooling efficiency at room temperature for KPb_2Cl_5 crystal has also been investigated by making use of excitation spectra. Figure 7(a) shows the excitation spectra collecting the luminescence at 1035 nm (at the end of the cooling zone) and at two different pumping irradiances, 1W and 250 mW. Figure 7(b) displays the normalized difference of both spectra. It is worthy to mention that except for the region around the main absorption peaks where an accurate difference is difficult to obtain (due to saturation effects in the spectrum taken at high irradiances), the difference shows, as in the case mentioned above for glass samples, a broad band peaking around 1010 nm which covers the spectral range where cooling occurs. A more detailed picture of this effect is shown in fig. 8 where the difference between excitation spectra, fig. 8(b), can be compared with the behavior of the normalized deflection amplitude fig. 8(a).

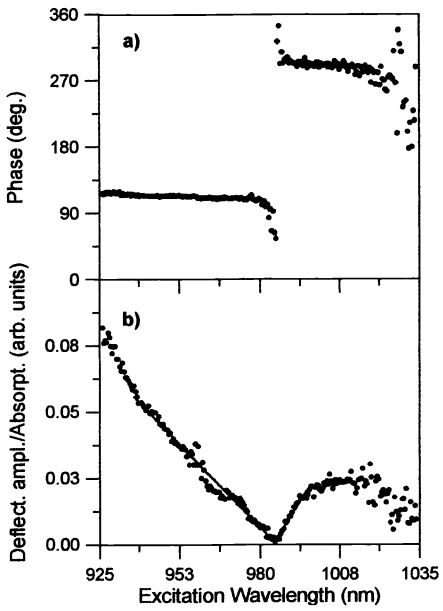

Figure 5. (a) Phase of the photothermal deflection signal and (b) photothermal deflection amplitude (normalized by the incident laser power) divided by the absorption of the KPb_2Cl_5 crystal.

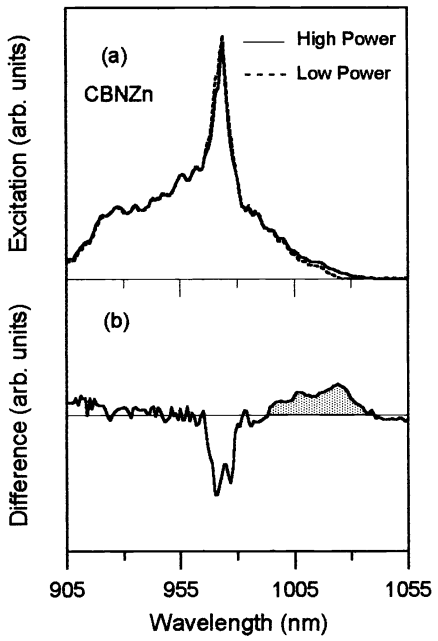

Figure 6. (a) High power (solid line) and low power (dashed line) excitation spectra recorded at 1040 nm and 225 K in CNBZn glass. (b) Difference between both spectra. The shaded area corresponds to the cooling luminescence.

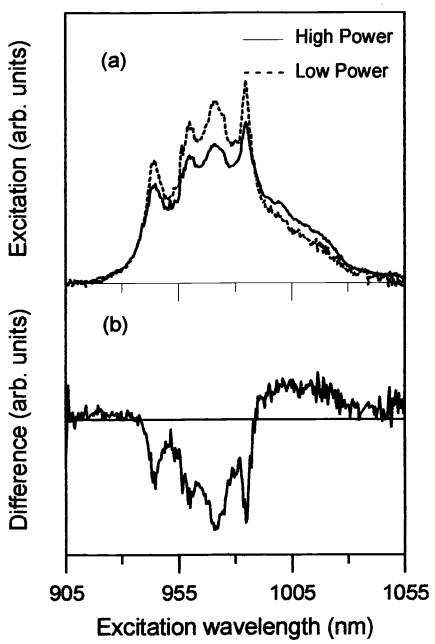

Figure 7. (a) High power (solid line) and low power (dashed line) excitation spectra recorded at 1035 nm in KPb_2Cl_5 crystal. (b) Difference between both spectra.

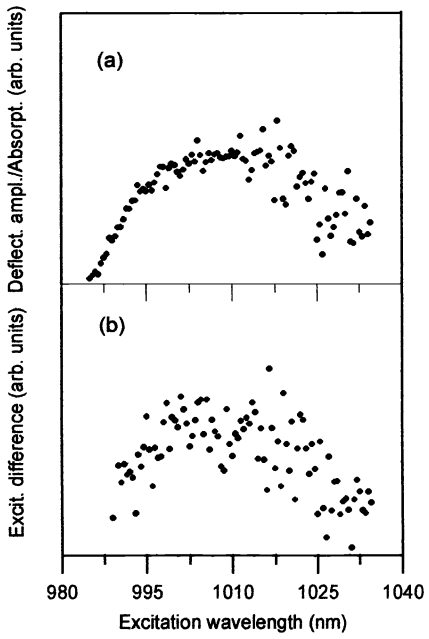

Figure 8. Detail of the normalized deflection amplitude (a) and difference between excitation spectra (b).

4. A MODEL FOR ANTI-STOKES COOLING

The spectroscopic results analyzed above clearly reveal that the cooling range is restricted to a narrow spectral region. Moreover, the thermal dependence of the additional fluorescence which appears in the excitation spectra as a consequence of cooling, makes clear that the cooling efficiency is a function of temperature.

In this section we present a simplified theoretical model which has been worked out by some of the authors [9]. The model gives, as far as we know for the first time, an explanation about the origin of laser cooling in Yb^{3+} doped glasses as well as its temperature dependence. Beginning with an ytterbium ion in its ground state a second order process which consists in the absorption of an incident photon and a phonon of the glass matrix, drives the ion to the excited state from which a photon of higher energy can be released. The cycle of this kind of processes gives rise to the observed cooling.

In order to estimate the probability per unit time of such a second order process let us consider our physical system described by the Hamiltonian:

$$H = H^{\text{ion}} + H^{\text{ph}} + H^{\text{em}} + V^{\text{ion-em}} + V^{\text{ion-ph}} \tag{6}$$

where

$$H^{\text{ion}} = \hbar\omega_0 a^+ a$$

is the Hamiltonian of the ion electronic levels being $\hbar\omega_0$ the energy difference between the optically active energy levels of the dopant ion (considered as a two level ion) and $a^+(a)$ the creation (annihilation) operator of an electronic excitation;

$$H^{\text{ph}} = \sum_q \hbar\omega_q b_q^+ b_q$$

is the phonon field Hamiltonian with $b_q^+(b_q)$ the creation (annihilation) operator of a phonon in mode q;

$$H^{\text{em}} = \hbar\omega_{\text{L}} c^+ c$$

is the electromagnetic laser field with ω_L the laser frequency and $c^+(c)$ the creation (annihilation) operator of a photon;

$$V^{\text{ion-em}} = -\hat{e}_{\text{L}} \cdot \mu \sqrt{\frac{\hbar\omega_{\text{L}}}{2\varepsilon_0 V}} \left(a^+ + a\right)\left(c^+ + c\right)$$

is the ion-photon interaction Hamiltonian, being $\hat{e}_{\text{L}}$ the polarization vector of the photon, μ the dipole moment of the electronic transition, ε_0 the vacuum permitivity, and V the interacting volume;

$$V^{\text{ion-ph}} = \Lambda \sqrt{\frac{\hbar\omega_q}{2\rho v^2}}\, a^+ a \left(b_q - b_q^+\right)$$

is the ion-phonon interaction Hamiltonian, where Λ is the ion-phonon coupling constant, v is the sound velocity, and ρ the mass density.

The probability per unit time of a process in which the ion in its ground state absorbs an incident photon and a phonon and goes up to the excited state can be evaluated by using the perturbation theory. This kind of processes appears in the second order term of the perturbation expansion. The transition probability is given by the Fermi's Golden Rule

$$w = \sum_f w_{fi} = \frac{2\pi}{\hbar} \sum_f \left|t_{fi}\right|^2 \delta\left(E_f - E_i\right) \tag{7}$$

where E_i and E_f are respectively the initial and final energies of the system. The t matrix admits a perturbative expansion given by

$$t_{fi} = \langle f|V_{\text{int}}|i\rangle + \sum_m \frac{\langle f|V_{\text{int}}|m\rangle\langle m|V_{\text{int}}|i\rangle}{E_i^{\text{T}} - E_m^{\text{T}}} + \sum_{m,n} \frac{\langle f|V_{\text{int}}|m\rangle\langle m|V_{\text{int}}|n\rangle\langle n|V_{\text{int}}|i\rangle}{\left(E_i^{\text{T}} - E_m^{\text{T}}\right)\left(E_i^{\text{T}} - E_n^{\text{T}}\right)} + \cdots \quad (8)$$

with $V_{\text{int}} = V^{\text{ion-em}} + V^{\text{ion-ph}}$. The summation on *m* and *n* includes all the intermediate phonon and photon states.

We are interested in the calculation of the transition probability between initial $|i\rangle = |a,n,n_q\rangle$ and final $|f\rangle = |b,0,0\rangle$ states of our system, where the first ket element, *a,* refers to the ion state, the second one, *n,* to the photon occupation number, and the third one, to the phonon occupation number. This type of processes only appears at second order in the perturbation theory expansion of the *t* matrix, and the calculation, though easy, is too lengthy to be presented here and will be given elsewhere. The contribution of these processes to the transition probability is given by

$$w = \sum_f w_{fi} = \frac{2\pi}{\hbar}\left(\frac{\omega_0}{\omega_{\text{L}}}\right)^2 \sum_q \left(\frac{gD_q}{\hbar\omega_q}\right)^2 n\, n_q\, \delta\left(-\hbar\omega_0 + \hbar\omega_{\text{L}} + \hbar\omega_q\right) \quad (9)$$

where

$$g^2 = \frac{\left(\hat{e}_{\text{L}} \cdot \boldsymbol{\mu}\right)^2}{2\varepsilon_0 V}\hbar\omega_{\text{L}}\,, \text{ and} \qquad D_q^2 = \Lambda^2 \frac{\hbar\omega_q}{2\rho v^2} \quad (10)$$

In order to evaluate the summation on the phonon modes in (9), we must introduce the phonon density of states, *P(E)*. In terms of this distribution function, the transition probability can be expressed in the following way

$$w = \frac{2\pi}{\hbar}\left(\frac{\omega_0}{\omega_{\text{L}}}\right)^2 g^2 n \frac{\Lambda^2}{2\rho v^2} \int_{E_{min}}^{E_{max}} dE\, P(E) \frac{n(E)}{E}\, \delta(-\hbar\omega_0 + \hbar\omega_{\text{L}} + E) \quad (11)$$

which after integration gives

$$w = \pi \frac{\left(\hat{e}_{\text{L}} \cdot \boldsymbol{\mu}\right)^2 \Lambda^2 n}{2\varepsilon_0 V \rho v^2} \frac{\omega_0^2}{\omega_{\text{L}}} \frac{P\left(\hbar\omega_0 - \hbar\omega_{\text{L}}\right) f\left(\hbar\omega_0 - \hbar\omega_{\text{L}}\right)}{\hbar\omega_0 - \hbar\omega_{\text{L}}}, \quad \text{if } \hbar\omega_0 > \hbar\omega_{\text{L}} \quad (12)$$

In this expression, *n* is the photon density of the incident beam, *f* is the Bose-Einstein function, and *P* is the phonon density of states.

Raman and infrared absorption measurements performed on CNBZn glass powder showed a complex broad band centered around 300 cm^{-1} which may be attributed to Cd-Cl (250 cm^{-1}) and Cd-F (370 cm^{-1}) vibrational modes. Therefore, a gaussian-like function centered around 370 cm^{-1}, the higher energy band, was selected as a plausible function for the phonon density of states. In order to avoid a divergence in the transition probability at the resonance $\hbar\omega_0 = \hbar\omega_L$, the gaussian function was scaled by the Debye distribution function in such a way that at low phonon energies the distribution function resembles the Debye one, whereas it is close to a gaussian at the center of the distribution. This choice avoids the introduction of a cut-off at low phonon frequencies and therefore the introduction of unnecessary parameters in the model. The form of the selected function is

$$P(E) = C E^2 \exp\left[-\left(\frac{E - \bar{E}}{\Gamma}\right)^2\right] \quad (13)$$

where $E=\hbar\omega_0-\hbar\omega_L$ is the phonon energy, $\overline{E}=\hbar\overline{\omega}$ is the energy at the center of the distribution, Γ its width (~100 cm^{-1}), and C an adequate normalization constant.

In the case of BIG glass, on the basis of Raman measurements in similar compounds, the center of the gaussian function representing the phonon density of states was taken at 510 cm^{-1}, and Γ~100 cm^{-1}.
With this distribution function, expression [12] becomes

$$w = C\pi \frac{(\hat{e}_L \cdot \mu)^2 \Lambda^2 n}{2\varepsilon_0 V \rho v^2} \frac{(\hbar\omega_0 - \hbar\omega_L)\omega_0^2}{\omega_L} \exp\left[-\left(\frac{\hbar\omega_0 - \hbar\omega_L - \hbar\overline{\omega}}{\Gamma}\right)^2\right] f(\hbar\omega_0 - \hbar\omega_L) \qquad (14)$$

if $\hbar\omega_0>\hbar\omega_L$.

The intensity of the additional fluorescence is proportional to the population excess of the fluorescent level produced by these second order processes and the probability for radiative transition to the ground state. Therefore, taking the emitting level QE as one, the temperature dependence of the integrated cooling fluorescence can be determined by comparing the experimental data with the expression

$$I(T) \sim \int w(\omega_L, T) d\omega_L \qquad (15)$$

We can integrate on the absorbed phonon energy, $E = \hbar\omega_0 - \hbar\omega_L$, at each pumping frequency. The lower limit of the integral is zero whereas we can take the Debye energy representing the maximum phonon energy present in the material as the upper limit. In any case, the value of the integral is quite insensitive to the upper limit as long as we are far from $E = \hbar\omega_0$, as it is the case.

Substituting expression (14) in (15) gives

$$I(T) \sim \int_{\hbar\omega_0 - \hbar\omega_D}^{\hbar\omega_0} \frac{\omega_0 - \omega_L}{\omega_L} \exp\left[-\left(\frac{\omega_0 - \omega_L - \overline{\omega}}{\Delta\omega}\right)^2\right] f(\hbar\omega_0 - \hbar\omega_L) d\omega_L \qquad (16)$$

where $\hbar\overline{\omega} = \overline{E}$ y $\hbar\Delta\omega = \Gamma$. Introducing the variable $x = \omega_0 - \omega_L$ we finally obtain:

$$I(T) \sim \int_0^{\omega_D} \frac{x}{\omega_0 - x} \exp\left[-\left(\frac{x - \overline{\omega}}{\Delta\omega}\right)^2\right] \frac{1}{\exp(x/k_B T) - 1} dx, \qquad (17)$$

where ω_D is the Debye frequency.

In order to compare the results of the numerical evaluation of the integrated intensity (expression (17)) with the experimental data, we have included the effect of inhomogeneous broadening by adding a constant background which is not dependent on temperature:

$$i(T) = a + b\, I(T). \qquad (18)$$

where *I(T)* is given by (17), and *a* and *b* are constants.

5. DISCUSSION

Figure 9 shows the integrated intensity of the cooling fluorescence peak as a function of temperature for both glasses. The continuous line is the fitting to the theoretical model given by eq. (18). The only parameters used in this fitting are the constants in (18) accounting for the inhomogeneous broadening.

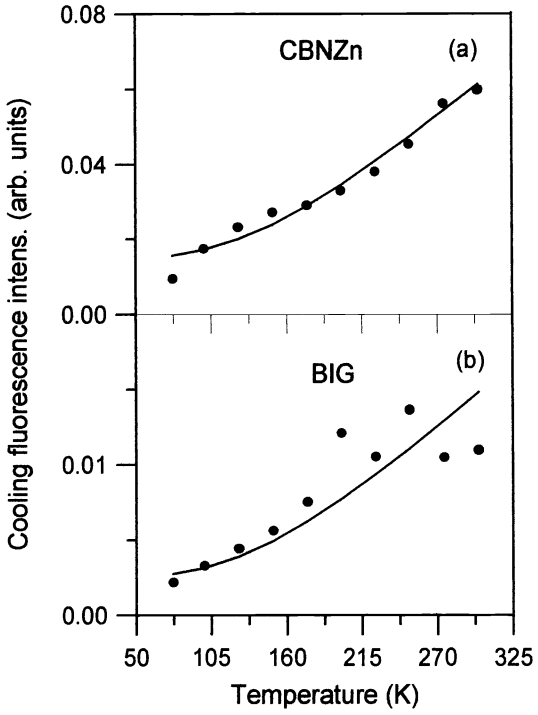

Figure 9. Experimental cooling fluorescence integrated intensities as a function of temperature (dots) and fitting to equation (18) (solid line) for CNBZn glass (a) and BIG glass (b)

As we can see, the agreement between experimental results and theory is very good and supports not only the model hypothesis about the kind of processes involved, but also the distribution function used for the phonon energies. Moreover, if we compare the relative integrated intensities at different temperatures we can have a real picture about the temperature dependence of the cooling efficiency of the material. Our experimental results in these glasses show it is possible to cool an internal volume from room temperature down to 70 K but with a penalty of about a 20 % in the cooling efficiency (cooling efficiency is defined as the ratio of the integrated cooling fluorescence peak to the integrated intensity of the high power excitation spectrum without the cooling peak contribution).

It is worthy to mention the quite good agreement between the room temperature cooling efficiencies obtained by using photothermal QE measurements and the ones obtained by measuring the fluorescence excess from the excitation spectra. In the former case an efficiency of 2 and 0.6 % respectively were found for CNBZn and BIG glasses, whereas in the second case values of 3 and 1 % respectively were obtained for the same samples. Referring to KPb_2Cl_5 crystal both techniques gave the same result of 0.2 %. However, account taken of the lesser density of ytterbium ions in the crystal (~ 10 times less than in glasses) and its smaller size we could estimate its cooling efficiency to be about 2%.

6. SUMMARY

Laser-induced internal cooling in a fluoride glass, a fluorochloride glass, and a chloride crystal has been demonstrated at room temperature by making use of photothermal deflection spectroscopy and excitation and absorption spectroscopies.

The cooling efficiency of these systems has been evaluated at room temperature by using two different experimental techniques. The results from both techniques are in good agreement for all the measured compounds. The fluorochloride glass shows a slightly higher efficiency.

The cooling efficiency has been evaluated in both glasses from 77 K to room temperature from the high and low power excitation spectra. The efficiency at 77 K falls to about 20% of its value at room temperature.
The experimental results are in good agreement with the predictions of a theoretical model based on the hypothesis of a second order process for the cooling mechanism.

In conclusion, we can state that anti-Stokes cooling in solids is strongly dependent on the phonon density of states of the system as well as on the ion-phonon coupling constant. Appropriate values in any or both parameters may lead to the cooling process in presence of a high enough photon irradiance.

ACKNOWLEDGEMENTS

This work has been supported by the Basque Country University (UPV 13525/2001), Spanish Government MCYT (Ref. MAT2000-1135 and BFM2000-0352), and Basque Country Government (PI99-95).

REFERENCES

[1] P. Pringsheim, "Zwei Bemerkungen über den Unterschied von Lumineszenz -und Temperaturstrahlung", *Z. Phys.* **57**, pp. 739-746, 1929.

[2] R. I. Epstein, M. I. Buchwald, B. C. Edwards, T. R. Gosnell, and C. E. Mungan, "Observation of laser-induced fluorescent cooling of a solid", *Nature* **377**, pp. 500-503, 1995.

[3] J. Fajardo, G. H. Sigel Jr., B. C. Edwards, R. I. Epstein, T. R. Gosnell, and C. E. Mungan, "Electrochemical purification of heavy metal fluoride glasses for laser-induced fluorescent cooling applications", *J. Non-Cryst. Solids* **213**, pp. 95-100, 1997.

[4] G. Lei, J. E. Anderson, M. I. Buchwald, B. C. Edwards, R. I. Epstein, M. T. Murtagh, and G. H. Siegel Jr., "Spectroscopic evaluation of Yb^{3+}-doped glasses for optical refrigeration", *IEEE J. of Quantum Electron.* **34**, pp. 1839-1845, 1998.

[5] M. T. Murtagh, G. H. Siegel Jr., J. Fajardo, B. C. Edwards, and R. I. Epstein, "Compositional investigation of Yb^{3+}-doped heavy metal fluoride glasses for laser-induced fluorescent cooling applications", *J. Non-Cryst. Solids* **257**, pp. 207-211, 1999.

[6] C. E. Mungan, M. I. Buchwald, B. C. Edwards, R. I. Epstein, and T. R. Gosnell, "Laser cooling of a solid by 16 K starting from room temperature", *Phys. Rev. Lett.* **78**, pp. 1030-1033, 1997.

[7] X. Luo, M. D. Eisaman, and T. R. Gosnell, "Laser cooling of a solid by 21 K starting from room temperature", *Opt. Lett.* **23**, pp. 639-641, 1998.

[8] T. R. Gosnell, "Laser cooling of a solid by 65 K starting from room temperature", *Opt. Lett.* **24**, pp. 1041-1043, 1999.

[9] J. Fernández, A. Mendioroz, A. J. García, R. Balda, and J. L- Adam, "Anti-Stokes laser-induced internal cooling of Yb^{3+}-doped glasses", *Phys. Rev. B* **62**, pp.3213-3217, 2001.

[10] S. R. Bowman and C. E. Mungan, "New materials for optical cooling", *Appl. Phys. B* **71**, pp. 807-811, 2000.

[11] R. I. Epstein, J. J. Brwn, B. C. Edwards, and A. Gibbs, "Measurements of optical refrigeration in ytterbium-doped crystals", *J. Appl. Phys.* **90**, pp. 4815-4819, 2001.

[12] J. L. Clark and G. Rumbles, "Laser cooling in the condensed phase by frequency up-conversion", *Phys. Rev. Lett.* **76**, pp. 2037-2040, 1996.
[13] E. Finkeiβen, M. Potemski, and P. Wyder, "Cooling of a semiconductor by luminescence up-conversion", *Appl. Phys. Lett.* **75**, pp. 1258-1260, 1999.
[14] G. Lamouche, P. Lavallard, R. Suris, and R. Grousson, J. "Low temperature laser cooling with a rare-earth doped glass", *Appl. Phys.* **84**, pp. 509-516, 1998.
[15] S. R. Bowman, "Lasers without internal heat generation", *IEEE J. Quantum Electron.* **35**, pp. 115-121, 1999.
[16] S. R. Bowman and C. E. Mungan, "Selecting materials for radiation balanced lasers", *Advanced Solid State Lasers, OSA Trends in Optics and Photonics Series*, pp. 156-158,1999
[17] J. Etxebarria and J. Fernández, "Photoacoustic spectra of transparent solids with localised absorbing centres", *J. Phys. C: Solid State Phys.*, **16**, pp. 3803-3811, 1983.
[18] A. Salazar, A. Sánchez-Lavega, and J. Fernández, "Thermal diffusivity measurements on solids using collinear mirage detection", *J. Appl. Phys.* **74**, pp. 1539-1547, 1993.
[19] W. B. Jackson, N. M. Amer, A. C. Boccara, and D. Fournier, "Photothermal deflection spectroscopy and detection", *Appl. Optics* **20**, pp. 1333-1344, 1981.